


Modeling Temperature-Dependent Electron Thermal Diffuse Scattering via Machine-Learned Interatomic Potentials and Path-Integral Molecular Dynamics

Dennis S. Kim^{✉,*}, Michael Xu[✉], and James M. LeBeau^{✉,†}

Department of Materials Science and Engineering, Massachusetts Institute of Technology, Cambridge, Massachusetts 02139, USA

 (Received 7 March 2023; revised 12 January 2024; accepted 25 January 2024; published 22 February 2024)

Electron thermal diffuse scattering is shown to be sensitive to subtle changes in atomic vibrations and shows promise in assessing lattice dynamics at nanometer resolution. Here, we demonstrate that machine-learned interatomic potentials (MLIPs) and path-integral molecular dynamics can accurately capture the potential energy landscape and lattice dynamics needed to describe electron thermal diffuse scattering. Using SrTiO₃ as a test bed at cryogenic and room temperatures, we compare electron thermal diffuse scattering simulations using different approximations to incorporate thermal motion. Only when the simulations are based on quantum mechanically accurate MLIPs in combination with path-integral molecular dynamics that include nuclear quantum effects is there excellent agreement with experiments.

DOI: [10.1103/PhysRevLett.132.086301](https://doi.org/10.1103/PhysRevLett.132.086301)

Thermally excited atomic motion governs many thermo-physical properties of solid-state materials with macroscopic consequences on phase transitions, physical, chemical, electronic, and optoelectronic material properties [1–4]. Modeling this correlated atomic motion is often considered within the harmonic approximation (first-order terms of the Taylor expansion) of the crystal potential energy surface. At finite temperatures, however, many solids behave anharmonically, in part, as a consequence of phonon-phonon interactions. Further, the higher-order terms describing the energy surface lead to finite phonon lifetimes or energy broadening, which are essential to describe thermal transport properties [5]. In addition, nuclear quantum effects are often neglected, which includes the zero-point energy and atomic tunneling [6].

Infrared, Raman, neutron, x-ray, and electron scattering methods have made significant progress in measuring phonon behavior in bulk materials, each with its own limitations. Infrared and Raman scattering techniques, for instance, are typically limited to only symmetry-allowed modes, while neutron and x-ray methods generally require bulk samples and instrumentation only available at national facilities. Meanwhile, recent advances in electron energy loss spectroscopy in scanning transmission electron microscopy (STEM) enable direct measurement of vibrational properties with nanometer resolution [7], but require specialized instrumentation and are most sensitive to higher-energy phonon modes [8,9].

Electron thermal diffuse scattering (eTDS) in parallel beam electron diffraction [10–13], for example, encodes the phonon dispersion relationships into nonuniform background features that arise due to partially coherent displacements of atoms away from equilibrium positions [14–16]. To compare theory and experiment in ultrathin single-layer materials, for example, analytical kinematical electron

scattering calculations have been used as was applied in x-ray studies [17]. Moreover, these prior studies have largely relied on harmonic phonons without including cubic and quartic terms in the crystal Hamiltonian (anharmonicity) and nuclear quantum effects [12,13,18]. While kinematical models are in agreement with ultrathin samples, fully quantifying analysis of eTDS has been stymied by the difficulties in data interpretation resulting from strong dynamical scattering and other inelastic scattering processes (e.g., plasmon losses).

For comparisons with experiment, electron scattering simulations must accurately describe scattering within samples that are tens to hundreds of nm thick, beyond the limits of first-principles calculations [18–20]. This is largely achieved using dynamical frozen phonon multislice simulations that are the workhorse to model the effect of thermal vibrations on scattering [18,21–25]. Further, these frozen phonon simulations are in excellent agreement with quantum mechanically exact methods such as the quantum excitation potential method (QEP) [26]. Usually, however, only the Einstein approximation (uncorrelated thermal displacements) is considered. Although this approximation has been shown to be in excellent agreement with imaging experiments [27,28], it does not accurately reproduce the diffuse scattering details such as streaking or Brillouin zone boundary features. In contrast, frozen phonon simulations backed by the stochastic temperature-dependent effective potential method showed feasibility for predicting accurate electron diffraction patterns, but only for Si where anharmonicity and nuclear quantum effects are not the major contributions to capture lattice dynamics at room temperature [29].

MLIPs, which are used as classical molecular dynamic potentials with local descriptors, have been shown to be capable of accurately mapping the potential energy surface and predicting thermal properties of materials while

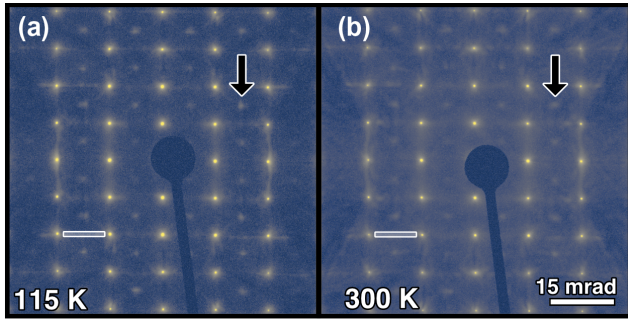


FIG. 1. High-dynamic range spot diffraction patterns including thermal diffuse scattering (TDS) of [110] SrTiO₃ at 115 (a) and 300 K (b). Black arrows indicate the BZ R -point intensity, and the white boxes highlight the linear thermal diffuse features.

circumventing the size constraints in first-principles calculations [30–35]. Although there are effective ways of validating the MLIPs against the input density functional theory (DFT) data, MLIPs and the level of theory used to train MLIPs should accurately predict experimental observables. Atomic vibrations from MLIPs and DFT calculations are typically tested against simulated or experimental phonon dispersions, i.e., the frequency-wave vector relations, but assessing phonon energies and lifetimes at spatial scales relevant for modern nanoscale applications have proven difficult [7,36,37]. As such, validating the first-principles methods for training the MLIPs against the experimental observable of eTDS to understand atomic vibrations in complex systems exhibiting anharmonicity or nuclear quantum effects has so far been unexplored.

In this Letter, we show that applying state-of-the-art MLIPs and molecular dynamics simulations can accurately model electron diffuse scattering experiments to provide a quantifiable approach to characterize temperature-dependent lattice dynamics. Phonon anharmonicity and nuclear quantum effects are included through the use of these MLIPs with classical (ML-CMD) and path-integral molecular dynamics (ML-PIMD). Here, SrTiO₃ is chosen as a model system due to its anomalous anharmonic phonon softening with decreasing temperature, known strong electron-phonon coupling, an antiferrodistortive structural phase transition, and strong quantum fluctuation dependence [1,38–50]. Frozen phonon electron diffraction simulations backed by MLIPs-based thermal displacements are compared against parallel beam diffraction patterns captured from high-dynamic range methods. Only after accounting for the key contributions to thermal displacements are the calculations shown to be in excellent agreement with the experiments. This method is general and can complement other methods to understand changes in atomic motion caused by many-body interactions, defects, and/or finite-size effects in solid materials.

High dynamic range parallel beam diffraction patterns of cubic SrTiO₃ along [110] at 115 (a) and 300 K (b) are shown in Fig. 1. Patterns were acquired on flat regions

(approximately 40 nm thick) of polished single crystals of SrTiO₃ using energy-filtered parallel beam diffraction (see the Supplemental Material [51]). The linear features between Bragg reflections, such as indicated by the white box, are seen throughout the patterns and are the result of both thermal diffuse scattering and Kikuchi bands. An example of thermal diffuse linear features or streaks are enclosed with a white box in Fig. 1. In addition to the strong Bragg reflections (brightest features) and Kikuchi bands, the intensity also peaks at positions in between reflections for both temperatures, shown as black arrows in Fig. 1. Notably, these peaks occur at the R -point zone-boundary points, which should not be observed given the cubic $Pm\bar{3}m$ crystal structure, and these features are considerably sharper (narrower) at 115 K compared to 300 K. Specifically, the average full-width at half maximum of the R -point feature changed on average by 15.8% between 300 and 115 K. This is consistent with the trend in previous x-ray scattering experiments [45], and has been attributed to the temperature-dependent softening of the R -point phonon mode [2,45,46,66–68].

Before comparing multislice simulations that account for different theoretical approximations of atomic vibrations with experiments, we tested the accuracy of the machine-learned interatomic potentials for the highly anharmonic SrTiO₃. We examined the lattice dynamics simulations using the stochastic temperature-dependent effective potential method (sTDEP) comparing *ab initio* and quadratic spectral neighbor analysis potentials (qSNAP) potentials [30–32,69,70]. We calculated and compared the 0 K harmonic phonon energies, temperature-renormalized harmonic phonons (H_h), and higher-order anharmonic (H_a) terms in the crystal Hamiltonian. The atomic displacements were based on stochastic samplings of the canonical ensemble that followed the Planck distribution, which includes nuclear quantum effects [4,71]. All DFT calculations, subsequent phonon calculations, machine-learned interatomic potential fitting, classical and path-integral molecular dynamics (C/PIMD), and analysis were performed using the QUANTUM ESPRESSO [72–74], temperature-dependent effective potential method (TDEP) software package [75], materials machine learning (MAML) PYTHON package [76], a large-scale atomic-molecular massively parallel simulator (LAMMPS) package, i-PI a universal force-engine, respectively [77,78]. For more information on computational methods, see the Supplemental Material [51].

We find that the machine-learned interatomic potentials reliably reproduce the potential energy surface when comparing the energies, forces, phonon dispersions, and phonon spectral functions [51,79]. As shown previously, cubic-SrTiO₃ is anharmonically stabilized as evidenced by the imaginary frequencies in the 0 K harmonic approximation (gray dashed line) compared to predicted stable structures in anharmonically renormalized harmonic dispersions at 115 (blue solid line) and 300 K (red solid line)

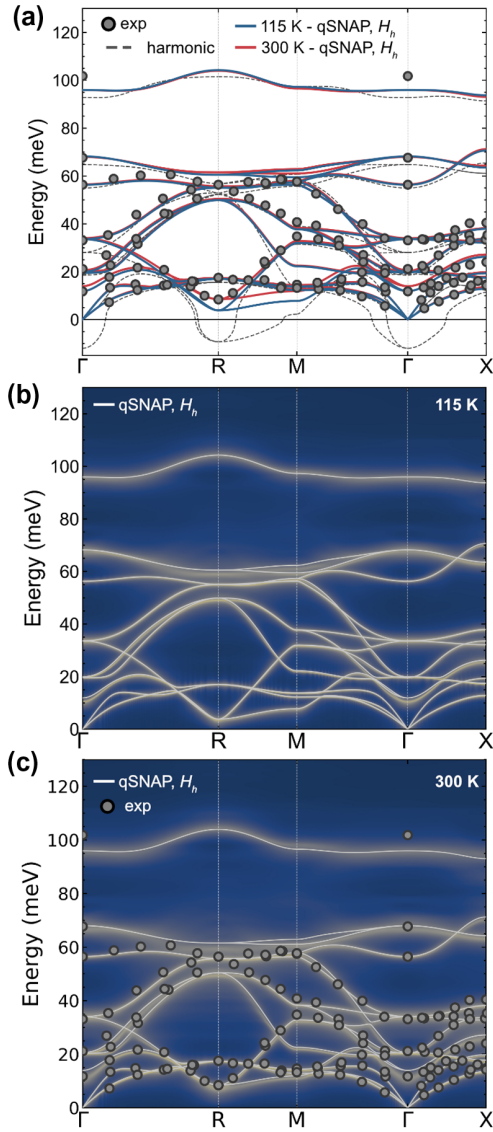


FIG. 2. Phonon dispersions along high-symmetry directions of SrTiO₃. Phonon energies were calculated using the temperature-dependent effective potential method using the qSNAP machine-learned interatomic potential (solid line) at 300 (red) and 115 K (blue). Inelastic neutron and Raman scattering experiments are shown as gray circle markers [81,82]. Phonon spectral functions were calculated using Supplemental Material [51], Eq. (3) at 115 (b) and 300 K (c). Harmonic phonon dispersions at 0 K are shown as a gray dashed line in (a)–(c). Inelastic neutron and Raman scattering experiments are shown as gray circles in (a) and (c) [81,82].

in Fig. 2(a). Although there are known inaccuracies in reproducing the band gap and other optical properties in complex oxides, using the Hubbard model (DFT + U) did not have a large effect on the phonon energies [80]. Moreover, the qSNAP potential can reproduce the effects of phonon anharmonicity beyond the renormalized harmonic frequencies as shown in the spectral functions in

Figs. 2(b)–2(c) and Fig. S1 [51]. Also, strong phonon thermal broadening is apparent in high-energy optical modes, and especially in soft-phonon modes near the *R*-point and the low energy Γ -point modes [Fig. 2(c)]. The qSNAP based phonon dispersions are consistent with previously published machine-learned potentials using the Gaussian approximation potential (GAP) and deep potential (DP) based deep neural network methods [50,79].

To understand the effects of different approximations on the thermal atomic displacements, we performed frozen-phonon multislice simulations for each. Equipped with an MLIP that accurately describes the finite-temperature potential energy surface and phonon dispersions from first principles, molecular dynamic simulations are performed to include the atomic interactions of higher-order terms in the Hamiltonian of simulated structures with thicknesses matching experiment. In the Supplemental Material, Fig. S2 shows a typical cell on the order of nanometers that is typically used for first-principles calculations, where MLIPs allow for similar accuracies of forces on atoms with the computational cost that allows for large simulation sizes that can approach tens to hundreds of nanometers in width and thickness [51]. This reduction in computational cost also allows for the addition of computing nuclear quantum effects. We introduce quantum effects through path-integral molecular dynamics methods. This method is based on Feynman’s path-integral formalism, where a quantum mechanical system is mapped to a classical ring-polymer based on beads. Atomic models of typical DFT supercell sizes, experimental supercells used in multislice simulations, and multiples beads used in PIMD of SrTiO₃ are shown in Fig. S2.c [6,51]. PIMD is different from the stochastic methods used to develop the MLIPs used in this Letter and allows for the system to evolve dynamically while capturing the correct physics of zero-point energy and quantum tunneling.

First, consider the Einstein approximation, which accounts for the correct magnitude of thermal displacements by assuming that atoms behave as independent harmonic oscillators. Although this approximation works well in simulating Kikuchi bands [83,84] and high-angle annular dark-field (HAADF) images [27], this simplified model does not capture the intricate collective behavior determined by the phonon dispersion relations as seen in the lack of strong intensities between Bragg reflections and at *R* points in the top left panel of Figs. 3(a)–3(b).

The collective behavior of atomic motion can be introduced by stochastically displacing atoms based on eigenfrequencies in phonon dispersion relations [71]. This approximation for a canonical ensemble has proven effective when fitting interatomic force constants or using this with strongly bonded solids with small yet anharmonic thermal displacements in Si [4,29]. The scattering simulations from atomic displacements from renormalized harmonic (H_h) simulations reproduce streaking features

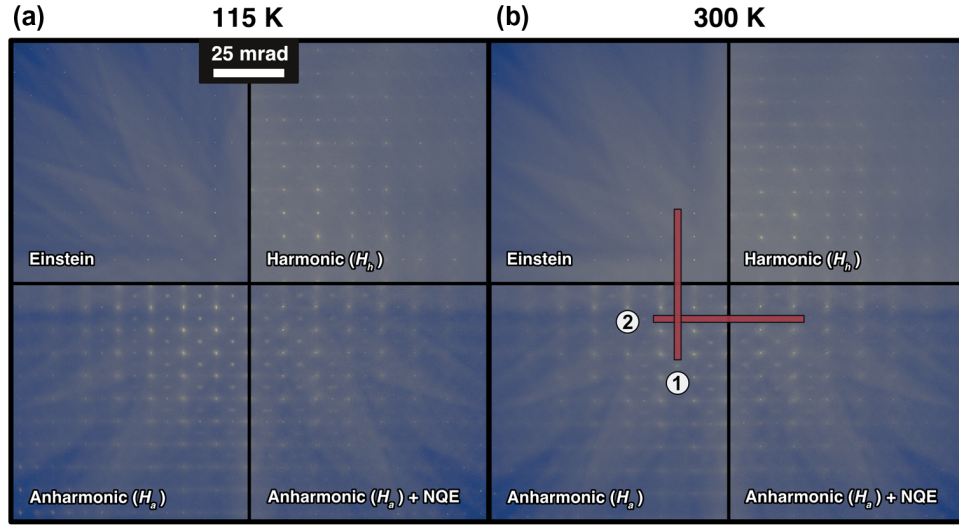


FIG. 3. Frozen phonon dynamical simulations using machine-learned interatomic potentials. Multislice simulations of parallel beam electron diffraction patterns of 32.5 nm thick SrTiO₃ slabs along the [110] zone axis at 115 (a) and 300 K (b). Einstein (top left), harmonic (H_h) approximated displacements using finite-temperature stochastic displacements using renormalized phonon dispersions (top right), anharmonicity included displacements from machine-learned interatomic potential based molecular dynamics (bottom left), and anharmonicity and nuclear quantum effects included displacements (bottom right) are shown for both temperatures. Line profiles of thermal diffuse scattering along the respective line in (1) and (2) are compared with experiments in Fig. 4.

[top right of Figs. 3(a) and 3(b)], but do not reproduce the strong intensities at R points represented as black arrows in the experimental data of Fig. 1. This approximation includes phonon dispersion information but lacks the higher-order terms of the crystal Hamiltonian and thus any information of phonon-phonon interactions. We observe strong intensities at these R points in patterns only when we include phonon anharmonicities through molecular dynamics simulations (bottom panel Fig. 4). We have also performed simulations for different thicknesses and found small variations in peak intensities, but all thicknesses retained the features at the R point and do not affect the analysis (Fig. S3 and S4 [51]).

When nuclear quantum effects, through path-integral methods, are added into the atomic motion, the diffuse scattering intensities are changed markedly in the vicinity of the Bragg reflections as shown in Fig. S8 [51] and are a better fit to experimental data. Line scans shown in Figs. 4(a) and 4(b) are from red boxes labeled (1) and (2) in Fig. 2(b), respectively. The top panels are from 115 K and the bottom from 300 K. Einstein (gray dashed line), anharmonic (H_a , colored dashed line), and anharmonic (H_a) with nuclear quantum effects (NQE) (colored solid line) are scaled to best fit experimental data (black circle markers in Fig. 4). The lack of correlated motion in the Einstein approximation does not reproduce the strong intensities between Bragg reflections leading to large errors when fit to the experimental data shown in Fig. 4. Along with the Einstein approximation simulations, thermal diffuse scattering simulations including phonon anharmonicities with and without nuclear quantum effects are

shown as solid and dashed lines, respectively. From these results, the majority of the strong features are explained by including the atomic vibrations resulting from the anharmonic phonon modes. Moreover, the fit to experiment improves further when including nuclear quantum effects, especially at cryogenic temperatures, where this contribution becomes more significant. The particular paths, (1 and 2), show how different areas of reciprocal space can be measured using the same zone axis. Path (1) crosses the M points in the Brillouin zone, compared to the paths across R points. The differences in phonon mode energies introduces variations in peak intensity and broadening in the thermal diffuse scattering.

To examine the effects of anharmonicity and nuclear quantum effects, we compare the peaks at the R point. The average R^2 for the least-square fits increase from 29.6% to 45.6% when nuclear quantum effects are included (Supplemental Material Fig. S6 [51]), whereas the Einstein approximation can only fit a constant intensity. The full width half maximum of the R point changes with temperature by 23.5% with and 88% without nuclear quantum effects. In other words, the ML-CMD based simulations overestimate the sharpness of the R -point features at 115 K. While the atomic motion in SrTiO₃ is known to show strong nuclear quantum effects [1], this has been previously difficult to accurately incorporate in electron microscopy simulations described above. In our analysis, we identified small errors between simulations and experiments as the energy filter does not exclude all inelastic processes. For a completely accurate quantitative analysis, it would be necessary to capture the intense

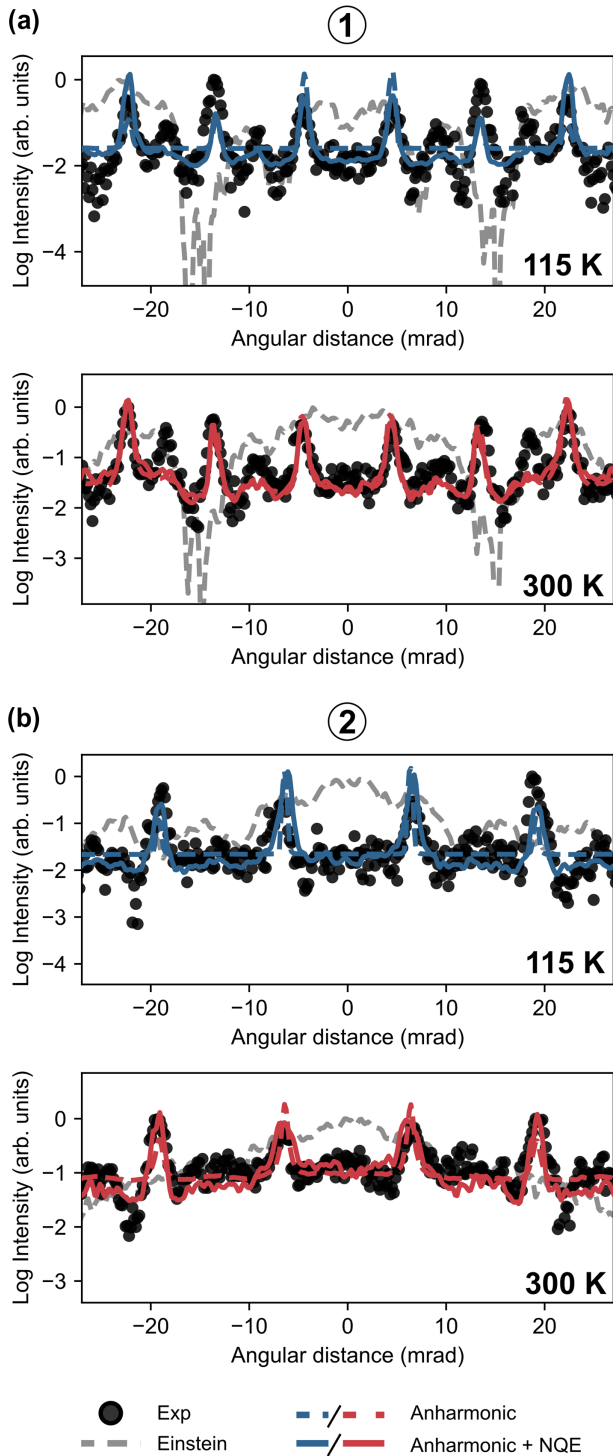


FIG. 4. Line profiles comparing experimental data from Fig. 1 and dynamical simulations are shown for (1) and (2) lines of Fig. 3. Experimental data are shown as black circle markers, the Einstein approximated simulations are shown as gray dashed lines, and anharmonic and anharmonic with nuclear quantum effects are shown as colored dashed and colored solid lines, respectively. Line profiles from 115 and 300 K are shown as blue and red, respectively.

central beam and account for low-energy inelastic plasmon scattering in the experimental data. This is beyond the scope of the current study and still an active area of research [85].

In conclusion, using SrTiO₃ as test bed, we have shown that the details of temperature-dependent electron thermal diffuse scattering distribution can validate the theoretical methods used to train MLIPs. These MLIPs with classical and path-integral molecular dynamics can account for anomalous, anharmonic phonons, and nuclear quantum effects. Moreover, the anomalous phonon soft-mode dynamics are predicted in the electron diffraction patterns and find much better agreement with simulations when phonon anharmonicity and nuclear quantum effects are included. For dynamical simulations, MLIPs are necessary for quantum mechanically accurate predictions due to larger-scale simulations that can account for realistic sample sizes in reasonable computational times. Overall, these results demonstrate that a combination of eTDS, DFT, and MLIPs opens a pathway to quantify atomic thermal behavior in materials.

We gratefully acknowledge support for this research from the Air Force Office of Scientific Research under Contract No. FA9550-20-0066. This work was carried out in part through the use of the MIT Characterization.nano facility. The authors acknowledge the MIT SuperCloud and Lincoln Laboratory Supercomputing Center for providing (HPC, database, consultation) resources that have contributed to the research results reported within this Letter.

*dennis.s.kim@icloud.com

†lebeau@mit.edu

- [1] W. Zhong and D. Vanderbilt, Effect of quantum fluctuations on structural phase transitions in SrTiO₃ and BaTiO₃, *Phys. Rev. B* **53**, 5047 (1996).
- [2] X. He, D. Bansal, B. Winn, S. Chi, L. Boatner, and O. Delaire, Anharmonic eigenvectors and acoustic phonon disappearance in quantum paraelectric SrTiO₃, *Phys. Rev. Lett.* **124**, 145901 (2020).
- [3] A. Löfgren, P. Zeiger, V. Kocevski, and J. Rusz, Influence of nuclear quantum effects on frozen phonon simulations of electron vortex beam HAADF-STEM images, *Ultramicroscopy* **164**, 62 (2016).
- [4] D. S. Kim, O. Hellman, J. Herriman, H. L. Smith, J. Y. Y. Lin, N. Shulumba, J. L. Niedziela, C. W. Li, D. L. Abernathy, and B. Fultz, Nuclear quantum effect with pure anharmonicity and the anomalous thermal expansion of silicon, *Proc. Natl. Acad. Sci. U.S.A.* **115**, 1992 (2018).
- [5] R. Peierls, Zur kinetischen theorie der wärmeleitung in kristallen, *Ann. Phys. (N.Y.)* **395**, 1055 (1929).
- [6] T. E. Markland and M. Ceriotti, Nuclear quantum effects enter the mainstream, *Nat. Rev. Chem.* **2**, 1 (2018).

- [7] C. A. Gadre, X. Yan, Q. Song, J. Li, L. Gu, H. Huyan, T. Aoki, S.-W. Lee, G. Chen, R. Wu, and X. Pan, Nanoscale imaging of phonon dynamics by electron microscopy, *Nature (London)* **606**, 292 (2022).
- [8] J. A. Hachtel, A. R. Lupini, and J. C. Idrobo, Exploring the capabilities of monochromated electron energy loss spectroscopy in the infrared regime, *Sci. Rep.* **8**, 5637 (2018).
- [9] O. L. Krivanek, T. C. Lovejoy, N. Dellby, T. Aoki, R. W. Carpenter, P. Rez, E. Soignard, J. Zhu, P. E. Batson, M. J. Lagos, R. F. Egerton, and P. A. Crozier, Vibrational spectroscopy in the electron microscope, *Nature (London)* **514**, 209 (2014).
- [10] Z. L. Wang, Thermal diffuse scattering in sub-angstrom quantitative electron microscopy—phenomenon, effects and approaches, *Micron* **34**, 141 (2003).
- [11] J. M. Zuo, J. Pacaud, R. Hoier, and J. C. Spence, Experimental measurement of electron diffuse scattering in magnetite using energy-filter and imaging plates, *Micron* **31**, 527 (2000).
- [12] M. R. Otto, J.-H. Pöhls, L. P. René de Cotret, M. J. Stern, M. Sutton, and B. J. Siwick, Mechanisms of electron-phonon coupling unraveled in momentum and time: The case of soft phonons in TiSe_2 , *Sci. Adv.* **7**, eabf2810 (2021).
- [13] L. P. René de Cotret, M. R. Otto, J.-H. Pöhls, Z. Luo, M. G. Kanatzidis, and B. J. Siwick, Direct visualization of polaron formation in the thermoelectric SnSe , *Proc. Natl. Acad. Sci. U.S.A.* **119**, e2113967119 (2022).
- [14] P. Debye, Interference of röntgen rays and heat motions, *Ann. Phys. (N.Y.)*, **348**, 49 (1913).
- [15] I. Waller, On the effect of thermal motion on the interference of x-rays, *Zeitschrift fur Physiotherapie* **17**, 398 (1923).
- [16] M. Born, Theoretical investigations on the relation between crystal dynamics and x-ray scattering, *Rep. Prog. Phys.* **9**, 294 (1942).
- [17] M. Holt, Z. Wu, H. Hong, P. Zschack, P. Jemian, J. Tischler, H. Chen, and T.-C. Chiang, Determination of phonon dispersions from x-ray transmission scattering: The example of silicon, *Phys. Rev. Lett.* **83**, 3317 (1999).
- [18] D. A. Muller, B. Edwards, E. J. Kirkland, and J. Silcox, Simulation of thermal diffuse scattering including a detailed phonon dispersion curve, *Ultramicroscopy* **86**, 371 (2001).
- [19] D. B. Durham, C. Ophus, K. M. Siddiqui, A. M. Minor, and D. Filippetto, Accurate quantification of lattice temperature dynamics from ultrafast electron diffraction of single-crystal films using dynamical scattering simulations, *Struct. Dyn.* **9**, 064302 (2022).
- [20] F. F. Krause, D. Bredemeier, M. Schowalter, T. Mehrrens, T. Grieb, and A. Rosenauer, Using molecular dynamics for multislice TEM simulation of thermal diffuse scattering in AlGaIn , *Ultramicroscopy* **189**, 124 (2018).
- [21] J. M. Cowley, A. F. Moodie, and IUCr, The scattering of electrons by atoms and crystals. I. A new theoretical approach, *Acta Crystallogr.* **10**, 609 (1957).
- [22] Z. L. Wang, The ‘Frozen-Lattice’ approach for incoherent phonon excitation in electron scattering. How accurate is it?, *Acta Crystallogr. Sect. A* **54**, 460 (1998).
- [23] A. Rosenauer, M. Schowalter, J. T. Titantah, and D. Lamoen, An emission-potential multislice approximation to simulate thermal diffuse scattering in high-resolution transmission electron microscopy, *Ultramicroscopy* **108**, 1504 (2008).
- [24] D. Van Dyck, Is the frozen phonon model adequate to describe inelastic phonon scattering?, *Ultramicroscopy* **109**, 677 (2009).
- [25] B. D. Forbes, A. J. D’Alfonso, S. D. Findlay, D. Van Dyck, J. M. Lebeau, S. Stemmer, and L. J. Allen, Thermal diffuse scattering in transmission electron microscopy, *Ultramicroscopy* **111**, 1670 (2011).
- [26] B. D. Forbes, A. V. Martin, S. D. Findlay, A. J. D’Alfonso, and L. J. Allen, Quantum mechanical model for phonon excitation in electron diffraction and imaging using a Born-Oppenheimer approximation, *Phys. Rev. B* **82**, 104103 (2010).
- [27] J. M. LeBeau, S. D. Findlay, L. J. Allen, and S. Stemmer, Quantitative atomic resolution scanning transmission electron microscopy, *Phys. Rev. Lett.* **100**, 206101 (2008).
- [28] A. Thust, High-resolution transmission electron microscopy on an absolute contrast scale, *Phys. Rev. Lett.* **102**, 220801 (2009).
- [29] X. Chen, D. S. Kim, and J. M. LeBeau, A comparison of molecular dynamics potentials used to account for thermal diffuse scattering in multislice simulations, *Ultramicroscopy* **244**, 113644 (2023).
- [30] Y. Zuo, C. Chen, X. Li, Z. Deng, Y. Chen, J. Behler, G. Csányi, A. V. Shapeev, A. P. Thompson, M. A. Wood, and S. P. Ong, Performance and cost assessment of machine learning interatomic potentials, *J. Phys. Chem. A* **124**, 731 (2020).
- [31] A. P. Thompson, L. P. Swiler, C. R. Trott, S. M. Foiles, and G. J. Tucker, Spectral neighbor analysis method for automated generation of quantum-accurate interatomic potentials, *J. Comput. Phys.* **285**, 316 (2015).
- [32] M. A. Wood and A. P. Thompson, Extending the accuracy of the SNAP interatomic potential form, *J. Chem. Phys.* **148**, 241721 (2018).
- [33] S. R. Xie, M. Rupp, and R. G. Hennig, Ultra-fast interpretable machine-learning potentials, *npj Comput. Mater.* **9**, 1 (2023).
- [34] J. Lahnsteiner and M. Bokdam, Anharmonic lattice dynamics in large thermodynamic ensembles with machine-learning force fields: CsPbBr_3 , a phonon liquid with cs rattlers, *Phys. Rev. B* **105**, 024302 (2022).
- [35] L. Ranalli, C. Verdi, L. Monacelli, G. Kresse, M. Calandra, and C. Franchini, Temperature-dependent anharmonic phonons in quantum paraelectric KTaO_3 by first principles and machinelearned force fields, *Adv. Quantum Technol.* **6**, 2200131 (2023).
- [36] J. D. Morrow, J. L. A. Gardner, and V. L. Deringer, How to validate machine-learned interatomic potentials, *J. Chem. Phys.* **158**, 121501 (2023).
- [37] X. Tian, X. Yan, G. Varnavides, Y. Yuan, D. S. Kim, C. J. Ciccarino, P. Anikeeva, M.-Y. Li, L.-J. Li, P. Narang, X. Pan, and J. Miao, Capturing 3D atomic defects and phonon localization at the 2D heterostructure interface, *Sci. Adv.* **7**, eabi6699 (2021).
- [38] J.-J. Zhou and M. Bernardi, Predicting charge transport in the presence of polarons: The beyond-quasiparticle regime in SrTiO_3 , *Phys. Rev. Res.* **1**, 033138 (2019).

- [39] T. Tadano and S. Tsuneyuki, *Ab initio* prediction of structural phase-transition temperature of SrTiO₃ from finite-temperature phonon calculation, *J. Ceram. Soc. Jpn.* **127**, 404 (2019).
- [40] Y. A. Abramov, V. G. Tsirelson, V. E. Zavodnik, S. A. Ivanov, and I. D. Brown, The chemical bond and atomic displacements in SrTiO₃ from X-ray diffraction analysis, *Acta Crystallogr. Sect. B* **51**, 942 (1995).
- [41] J.-J. Zhou, O. Hellman, and M. Bernardi, Electron-Phonon scattering in the presence of soft modes and electron mobility in SrTiO₃ perovskite from first principles, *Phys. Rev. Lett.* **121**, 226603 (2018).
- [42] R. A. Cowley, Lattice dynamics and phase transitions of strontium titanate, *Phys. Rev.* **134**, A981 (1964).
- [43] C. H. Perry, J. H. Fertel, and T. F. McNelly, Temperature dependence of the raman spectrum of SrTiO₃ and KTaO₃, *J. Chem. Phys.* **47**, 1619 (1967).
- [44] R. Wang, Y. Zhu, and S. M. Shapiro, Electron diffraction studies of phonon and static disorder in SrTiO₃, *Phys. Rev. B* **61**, 8814 (2000).
- [45] M. Holt, M. Sutton, P. Zschack, H. Hong, and T.-C. Chiang, Dynamic fluctuations and static speckle in critical x-ray scattering from SrTiO₃, *Phys. Rev. Lett.* **98**, 065501 (2007).
- [46] S. Ravy, D. Le Bolloc'h, R. Currat, A. Fluorasu, C. Mocuta, and B. Dkhil, SrTiO₃ displacive transition revisited via coherent x-ray diffraction, *Phys. Rev. Lett.* **98**, 105501 (2007).
- [47] H. B. Neumann, U. Rütt, J. R. Schneider, and G. Shirane, Origin of the critical scattering on two length scales in SrTiO₃: A high-energy synchrotron-radiation diffraction study, *Phys. Rev. B* **52**, 3981 (1995).
- [48] U. Rütt, A. Diederichs, J. R. Schneider, and G. Shirane, Depth dependence of strain, mosaicity and sharp component in the critical scattering of SrTiO₃, *Europhys. Lett.* **39**, 395 (1997).
- [49] H. Hünnefeld, T. Niemöller, J. R. Schneider, U. Rütt, S. Rodewald, J. Fleig, and G. Shirane, Influence of defects on the critical behavior at the 105 K structural phase transition of SrTiO₃: On the origin of the two length scale critical fluctuations, *Phys. Rev. B* **66**, 014113 (2002).
- [50] C. Verdi, L. Ranalli, C. Franchini, and G. Kresse, Quantum paraelectricity and structural phase transitions in strontium titanate beyond density functional theory, *Phys. Rev. Mater.* **7**, L030801 (2023).
- [51] See Supplemental Material at <http://link.aps.org/supplemental/10.1103/PhysRevLett.132.086301> for additional details of the experimental and computational methods, multislice simulations, and data analysis, which includes Refs. [52–65].
- [52] A. Togo and I. Tanaka, First principles phonon calculations in materials science, *Scr. Mater.* **108**, 1 (2015).
- [53] R. F. Egerton and S. C. Cheng, Measurement of local thickness by electron energy-loss spectroscopy, *Ultramicroscopy* **21**, 231 (1987).
- [54] K. Evans and R. Beanland, High dynamic range electron imaging: The new standard, *Microsc. Microanal.* **20**, 1601 (2014).
- [55] J. Madsen and T. Susi, The abTEM code: Transmission electron microscopy from first principles, *Open Res. Eur.* **1**, 24 (2021).
- [56] D. Chandler and P. G. Wolynes, Exploiting the isomorphism between quantum theory and classical statistical mechanics of polyatomic fluids, *J. Chem. Phys.* **74**, 4078 (1981).
- [57] I. R. Craig and D. E. Manolopoulos, Quantum statistics and classical mechanics: Real time correlation functions from ring polymer molecular dynamics, *J. Chem. Phys.* **121**, 3368 (2004).
- [58] M. Rossi, M. Ceriotti, and D. E. Manolopoulos, How to remove the spurious resonances from ring polymer molecular dynamics, *J. Chem. Phys.* **140**, 234116 (2014).
- [59] M. Ceriotti, M. Parrinello, T. E. Markland, and D. E. Manolopoulos, Efficient stochastic thermostating of path integral molecular dynamics, *J. Chem. Phys.* **133**, 124104 (2010).
- [60] L. Monacelli, R. Bianco, M. Cherubini, M. Calandra, I. Errea, and F. Mauri, The stochastic self-consistent harmonic approximation: Calculating vibrational properties of materials with full quantum and anharmonic effects, *J. Phys. Condens. Matter* **33**, 363001 (2021).
- [61] X. Gonze and C. Lee, Dynamical matrices, born effective charges, dielectric permittivity tensors, and interatomic force constants from density-functional perturbation theory, *Phys. Rev. B* **55**, 10355 (1997).
- [62] R. A. Cowley, Anharmonic crystals, *Rep. Prog. Phys.* **31**, 123 (1968).
- [63] J. Klarbring, O. Hellman, I. A. Abrikosov, and S. I. Simak, Anharmonicity and ultralow thermal conductivity in Lead-Free halide double perovskites, *Phys. Rev. Lett.* **125**, 045701 (2020).
- [64] O. Hellman and D. A. Broido, Phonon thermal transport in Bi₂Te₃ from first principles, *Phys. Rev. B* **90**, 134309 (2014).
- [65] N. Shulumba, O. Hellman, and A. J. Minnich, Lattice thermal conductivity of polyethylene molecular crystals from first-principles including nuclear quantum effects, *Phys. Rev. Lett.* **119**, 185901 (2017).
- [66] G. Shirane and Y. Yamada, Lattice-dynamical study of the 110°K phase transition in SrTiO₃, *Phys. Rev.* **177**, 858 (1969).
- [67] S. R. Andrews, X-ray scattering study of the r-point instability in SrTiO₃, *J. Phys. C* **19**, 3721 (1986).
- [68] R. J. Nelmes, P. D. Hatton, and H. Vass, Observations of a very large critical length scale in SrTiO₃, *Phys. Rev. Lett.* **60**, 2172 (1988).
- [69] O. Hellman, P. Steneteg, I. A. Abrikosov, and S. I. Simak, Temperature dependent effective potential method for accurate free energy calculations of solids, *Phys. Rev. B* **87**, 104111 (2013).
- [70] O. Hellman and I. A. Abrikosov, Temperature-dependent effective third-order interatomic force constants from first principles, *Phys. Rev. B* **88**, 144301 (2013).
- [71] N. Shulumba, O. Hellman, and A. J. Minnich, Intrinsic localized mode and low thermal conductivity of PbSe, *Phys. Rev. B* **95**, 014302 (2017).
- [72] P. Giannozzi *et al.*, QUANTUM ESPRESSO: A modular and open-source software project for quantum simulations of materials, *J. Phys. Condens. Matter* **21**, 395502 (2009).
- [73] P. Giannozzi *et al.*, Advanced capabilities for materials modelling with quantum ESPRESSO, *J. Phys. Condens. Matter* **29**, 465901 (2017).

- [74] J. P. Perdew, A. Ruzsinszky, G. I. Csonka, O. A. Vydrov, G. E. Scuseria, L. A. Constantin, X. Zhou, and K. Burke, Restoring the density-gradient expansion for exchange in solids and surfaces, *Phys. Rev. Lett.* **100**, 136406 (2008).
- [75] TDEP, <https://tdep-developers.github.io/tdep/> (accessed: 2023-9-14).
- [76] C. Chen, Y. Zuo, Yunxing, Q. Weike, Ji, and S. P. Ong, maml (materials machine learning), <https://github.com/materialsvirtuallab/maml> (2020).
- [77] A. P. Thompson, H. M. Aktulga, R. Berger, D. S. Bolintineanu, W. M. Brown, P. S. Crozier, P. J. in 't Veld, A. Kohlmeyer, S. G. Moore, T. D. Nguyen, R. Shan, M. J. Stevens, J. Tranchida, C. Trott, and S. J. Plimpton, LAMMPS—a flexible simulation tool for particle-based materials modeling at the atomic, meso, and continuum scales, *Comput. Phys. Commun.* **271**, 108171 (2022).
- [78] M. Ceriotti, J. More, and D. E. Manolopoulos, i-PI: A Python interface for *ab initio* path integral molecular dynamics simulations, *Comput. Phys. Commun.* **185**, 1019 (2014).
- [79] R. He, H. Wu, L. Zhang, X. Wang, F. Fu, S. Liu, and Z. Zhong, Structural phase transitions in SrTiO₃ from deep potential molecular dynamics, *Phys. Rev. B* **105**, 064104 (2022).
- [80] L. Zhang, B. Liu, H. Zhuang, P. R. C. Kent, V. R. Cooper, P. Ganesh, and H. Xu, Oxygen vacancy diffusion in bulk SrTiO₃ from density functional theory calculations, *Comput. Mater. Sci.* **118**, 309 (2016).
- [81] W. G. Stirling, Neutron inelastic scattering study of the lattice dynamics of strontium titanate: Harmonic models, *J. Phys. C* **5**, 2711 (1972).
- [82] J. L. Servoin, Y. Luspin, and F. Gervais, Infrared dispersion in SrTiO₃ at high temperature, *Phys. Rev. B* **22**, 5501 (1980).
- [83] R. F. Loane, P. Xu, and J. Silcox, Thermal vibrations in convergent-beam electron diffraction, *Acta Crystallogr. Sect. A* **47**, 267 (1991).
- [84] E. J. Kirkland, *Advanced Computing in Electron Microscopy* (Springer International Publishing, New York, 2020).
- [85] B. G. Mendis, An inelastic multislice simulation method incorporating plasmon energy losses, *Ultramicroscopy* **206**, 112816 (2019).